

Nonthermal warm dark matter limits from small-scale structure

Arka Banerjee,¹ Subinoy Das,² Anshuman Maharana,³ Ethan O. Nadler^{4,5} and Ravi Kumar Sharma^{2,*}


¹*Department of Physics, Indian Institute of Science Education and Research,
Homi Bhabha Road, Pashan, Pune 411008, India*

²*Indian Institute of Astrophysics, Bengaluru, Karnataka 560034, India*

³*Harish-Chandra Research Institute, A CI of Homi Bhabha National Institute,
Chhatnag Road, Jhansi, Prayagraj, Uttar Pradesh 211019, India*

⁴*Carnegie Observatories, 813 Santa Barbara Street, Pasadena, California 91101, USA*

⁵*Department of Physics and Astronomy, University of Southern California,
Los Angeles, California 90007, USA*

 (Received 30 May 2023; accepted 27 July 2023; published 15 August 2023)

We present small-scale structure constraints on sterile dark matter produced from a heavy mediator particle, inspired by models of moduli decay. Dark matter particles produced through this mechanism can contribute to the entire dark matter energy density but the particles have a nonthermal phase-space distribution; however, we show that the resulting linear matter power spectra can be mapped to effective thermal-relic warm dark matter models. This production mechanism is therefore subject to warm dark matter constraints from small-scale structure as probed by ultrafaint dwarf galaxy abundances and strong gravitational lensing flux ratio statistics. We use the correspondence to thermal-relic models to derive a lower bound on the nonthermal particle mass of 107 keV, at 95% confidence limits. These are the most stringent constraints derived on sterile dark matter produced via the heavy mediator decay scenario we consider.

DOI: [10.1103/PhysRevD.108.043518](https://doi.org/10.1103/PhysRevD.108.043518)

I. INTRODUCTION

The concordance Λ CDM model has been successful in describing the accelerated expansion of the Universe, as well as the evolution of perturbations on large scales, and fits most cosmological observations to date. Observations, including those from the cosmic microwave background, galaxy clustering, weak lensing, and Lyman- α measurements, imply that matter accounts for nearly 30 percent of the total energy density of the Universe today [1–3]. Most of this matter is *dark*; in the Λ CDM model, the dark matter is cold, meaning that its free-streaming effects are negligible. Although cold dark matter (CDM) is the simplest dark matter model that describes the data, potential tensions on small, nonlinear scales have been studied for several decades [4]. Historically, the “missing satellites” [5,6], “core-cusp” [7,8], and “too big to fail” [9] problems have received the most attention, while subtler measurements of galaxy diversity have been discussed in recent years [10].

Although most—if not all—of these potential tensions can be alleviated by baryonic physics, they have also inspired proposals for dark matter physics beyond the CDM paradigm. One classic model is that of warm dark matter (WDM), in which dark matter particles free stream on macroscopic scales of $\mathcal{O}(\text{kpc})$ or larger, imprinting an

observable suppression of small-scale structure relative to CDM [11,12]. WDM particle candidates, including sterile neutrinos, are often modeled with production mechanisms that yield a thermal phase-space distribution [13], which is strongly constrained by small-scale structure [14]. The mass varying dark matter scenario has been studied in [15]. Several production mechanisms that yield nonthermal distributions have also been proposed [16,17], although structure formation constraints on these models are also stringent [18–20].

Here, we study the impact of WDM production via the decay of a heavy scalar particle, inspired by models of moduli decay [21–23] where hot dark matter is produced from the moduli decay in the early Universe and contributes to a tiny fraction of total DM budget. Here, in this work, we instead address the scenario where the entire dark matter relic density is produced in a warm state via heavy scalar decay. We show that, despite its nonthermal phase-space distribution, this model yields linear matter power spectra that are indistinguishable from thermal-relic WDM but with a nontrivial mapping to a thermal-relic mass; this correspondence allows us to derive constraints on the nonthermal particle mass from state-of-the-art small-scale structure observations.

The small-scale structure limits we leverage were derived from Dark Energy Survey [24] and Pan-STARRS1 [25] observations of the Milky Way satellite galaxy population [26]. The population of observed satellites, and particularly

*ravi.sharma@iiap.res.in

the smallest “ultrafaint” dwarf galaxies detected nearby, has been used to place a lower limit on the abundance of low-mass ($\gtrsim 10^8 M_\odot$) subhalos orbiting the Milky Way [27]. In turn, this measurement constrains any dark matter physics that suppresses subhalo abundances, yielding a lower limit on the thermal-relic WDM particle mass of 6.5 keV at 95% confidence limits [18,20,28–31]. We also leverage strong gravitational lensing constraints. In particular, observations of flux ratio statistics of quadruply imaged quasars lensed by low-redshift elliptical galaxies have been used to derive constraints on WDM [32] and other dark matter physics [33–35]. Furthermore, Ref. [36] combined WDM constraints from strong lensing and Milky Way satellite galaxies set a lower limit on the thermal-relic mass of 9.7 keV at 95% confidence limits, which we use to derive the most stringent limit on our nonthermal production mechanism.

Importantly, both thermal-relic limits WDM we use, from Milky Way satellites alone and their combination with strong lensing, are marginalized over uncertainties in the properties of the respective systems and other nonlinear effects (e.g., galaxy formation physics in the satellite case and tidal stripping in the lensing case) that may affect the observables, ensuring that the constraints we derive here are conservative. Furthermore, because our model yields transfer functions that are nearly identical to thermal-relic WDM and does not introduce additional nonlinear physics, the constraints we derive by mapping to existing WDM limits are robust.

II. PRODUCTION MECHANISM AND PHASE-SPACE DISTRIBUTION

WDM scenarios are characterized by the primordial phase-space distribution of the warm species, which is determined by the production mechanism. We consider WDM produced from the decay of a heavy scalar, following Refs. [37–40]. In this scenario, the energy density of the universe is dominated by a cold, heavy species φ at early times; this epoch can be caused by perturbative reheating after inflation, or by moduli domination. φ then decays to the Standard Model sector and WDM particles. The decay channel to WDM particles is $1 \rightarrow 2$ with the production of two identical relativistic WDM particles. While the Standard Model sector thermalizes, the WDM particles are assumed to be sterile and thus do not thermalize. The model is natural to consider if one is interested in sterile dark matter produced from the decay of a heavy parent. Furthermore, it would also arise in cases where sterile dark matter is produced directly from the decay of the inflaton.

Thus, the WDM production rate is determined by the decay rate of φ and the branching ratio of the WDM channel. As φ decays, WDM particles are constantly produced, with momentum $m_\varphi/2$ at the time of production. The late-time momentum of a WDM particle is determined by redshifting its initial momentum. Because different WDM particles are produced at different times (but with

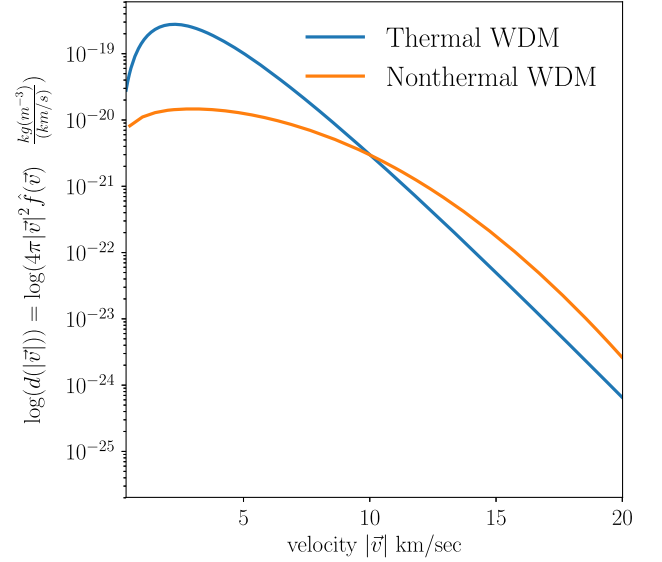


FIG. 1. Velocity distributions for thermal-relic WDM (blue) and our nonthermal WDM model (orange) at $z = 99$ for equal masses of 5 keV.

the same initial momentum), this redshifting effect leads to a nonthermal momentum distribution, as shown in Fig. 1.

The distribution function in our model is characterized by the mass of the heavy particle (m_φ), its decay rate, τ , and the branching ratio for decay to the WDM, B_{sp} . In particular, the momentum distribution of the WDM particles can be computed from the fact that, as a result of the decays, the comoving number density of φ falls off as $N(t) = N(0)e^{-t/\tau}$ with a branching ratio B_{sp} to the WDM particles. Once produced, the WDM particles free stream. The distribution function today was obtained in Ref. [40] as

$$g(\vec{q}) = \frac{32T_{\text{ncdm},0}^3}{\pi\hat{E}^3} \left(\frac{N(0)B_{\text{sp}}}{\hat{s}^3(\theta^*)} \right) \frac{e^{-\hat{s}^{-1}(y)}}{|\vec{q}|^3 \hat{H}(\hat{s}^{-1}(y))}. \quad (1)$$

Here, $T_{\text{ncdm},0}$ is the typical magnitude of the momentum of the particles and is given by

$$T_{\text{ncdm},0} = 0.418 \left(\frac{m_\varphi^2 \tau}{M_{\text{pl}}} \right)^{1/2} \frac{T_{\text{cmb}}}{(1 - B_{\text{sp}})^{1/4}} \equiv \zeta T_{\text{cmb}}. \quad (2)$$

In Eq. (1), $\hat{E} = m_\varphi/2$ is the energy of a WDM particle at the time of its production, $N(0)$ is the initial number density of φ particles, and $\hat{s}(\theta)$ is the scale factor as a function of the dimensionless time $\theta \equiv t/\tau$. The scale factor convention in Eq. (1) is such that $\hat{s} = 1$ at $\theta = 0$. Next, $\hat{s}(\theta^*)$ is its value at a fiducial value θ^* , at which most of the φ particles would have decayed (we take $\theta^* = 15$ for our computations), \hat{s}^{-1} is the functional inverse of the scale factor as a function of the dimensionless time, and $\hat{H} = \hat{s}'(\theta)/\hat{s}(\theta)$ is the dimensionless Hubble parameter. Finally, y is defined as

$$y = \frac{|\vec{q}|}{4} \hat{s}(\theta^*), \quad (3)$$

where \vec{q} is the momentum in units of the typical momentum magnitude of the WDM particles today, $T_{\text{ncdm},0}$. Note that \vec{q} is constrained such that

$$\frac{4}{\hat{s}(\theta^*)} < |\vec{q}| < 4. \quad (4)$$

We use the publicly available package CLASS [41,42] to study the effects of WDM in the above distribution. For this purpose, it is useful to consider the distribution function in Eq. (1) divided by $T_{\text{ncdm},0}^3$, i.e.

$$f(\vec{q}) = \frac{32}{\pi \hat{E}^3} \left(\frac{N(0) B_{\text{sp}}}{\hat{s}^3(\theta^*)} \right) \frac{e^{-\hat{s}^{-1}(y)}}{|\vec{q}|^3 \hat{H}(\hat{s}^{-1}(y))}. \quad (5)$$

We compare a typical momentum distribution in our model to that of thermal-relic WDM in Fig. 1. For the same value of ΔN_{eff} (the effective number of additional neutrino-like species) at the time of big bang nucleosynthesis (BBN), the nonthermal distribution is peaked at higher values of the momentum and is much broader than the thermal distribution. Note that the small-scale structure constraints we derive below imply that the allowed masses of WDM particles in our model are well below the temperature of the Universe during BBN.

Note that although naively $f(\vec{q})$ seems to depend on $N(0)$, the full expression is independent of $N(0)$ as long as we take the Universe to be completely matter dominated at the initial time [40]. On the other hand, changing the parameter B_{sp} scales the distribution function by an overall constant. For any value of the mass of the WDM particle, the CLASS package scales the distribution function so that Ω_{WDM} remains consistent with observations. Thus, values of B_{sp} are effectively sampled in our analysis. The other parameters in the distribution function are m_ϕ and τ . Motivated by high-scale inflation as the theory of the early Universe and the decay of the inflaton by perturbative GUT scale interactions, our interest is in $m_\phi \sim \mathcal{O}(10^{-6} M_{\text{pl}})$ and $\tau \sim \mathcal{O}(10^8/m_\phi)$. In the Appendix, we show that our results are insensitive to the precise values of these parameters.

III. LINEAR MATTER POWER SPECTRUM AND TRANSFER FUNCTION

We use a modified version of CLASS¹ [41,42] to generate linear matter power spectra for our nonthermal warm dark matter model. Throughout, we adopt the same cosmological parameters as Ref. [22]. For our WDM CLASS runs, we set $\omega_{\text{cdm}} = 0$. We include two non-CDM species, the first of which represents standard massless neutrinos, and the second of which is the WDM species with $N_{\text{ncdm}} = 2$ and

$\omega_{\text{ncdm}} = 0.12$. We fix the fiducial phase-space distribution parameters for our nonthermal WDM production mechanism following Ref. [22], with $B_{\text{sp}} = 0.0118$, $m_\phi = 10^{-6} M_{\text{pl}}$, and $\tau = 10^8/m_\phi$. We show in the Appendix that our results are not sensitive to the choices of these parameters; thus, our constraints are not sensitive to this choice.

The left panel of Fig. 2 shows the ratio of the linear matter power spectrum relative to CDM, hereafter referred to as the *transfer function*, for various nonthermal particle masses. In particular, we define

$$T^2(k) \equiv \frac{P(k)}{P_{\text{CDM}}(k)}. \quad (6)$$

We compare these transfer functions to the thermal-relic warm dark matter transfer function fit from Ref. [43]. Note that the relation between thermal-relic mass and cutoff scale derived from the Ref. [43] fitting function is inaccurate for sufficiently cold models, including those near our 95% confidence limits constraints; however, the shape of Ref. [43] transfer function cutoff is accurate [44,45]. Because the analyses we compare to also assumed the Ref. [43] functional form, which we only use as a means to map to effective thermal-relic models, this discrepancy does not affect our constraints.

The shape of the transfer function cutoff in our non-thermal model is clearly similar to that in thermal-relic warm dark matter. This allows us to construct a mapping between the models, following methodology similar to that in Refs. [36,46]. As illustrated in Fig. 2, we find that (for our fiducial cosmological parameters) the half-mode scale k_{hm} , defined by $T^2(k_{\text{hm}}) \equiv 0.25$, is related to the non-thermal particle mass via

$$k_{\text{hm}} = \left(3.3 + \frac{m_{\text{nonthermal}}}{1 \text{ keV}} \right) h \text{ Mpc}^{-1}, \quad (7)$$

where $m_{\text{nonthermal}}$ is our nonthermal particle mass.

As discussed in [43], the transfer function for thermal-relic WDM can be written as

$$T(k) = [1 + (\alpha k)^{2\nu}]^{-5/\nu}, \quad (8)$$

with $\nu = 1.12$ and

$$\alpha = 0.049 \left(\frac{m_{\text{WDM}}}{1 \text{ keV}} \right)^{-1.11} \left(\frac{\Omega_{\text{WDM}}}{0.25} \right)^{0.11} \left(\frac{h}{0.7} \right)^{1.22} h^{-1} \text{ Mpc}. \quad (9)$$

To obtain the relation between k_{hm} and m_{WDM} , we sample values of $m_{\text{WDM}} \in [3 \text{ keV}, 12 \text{ keV}]$, solve for their half-mode wave numbers k_{hm} using Eq. (8), and fit the results to obtain

$$k_{\text{hm}} = 12.5 \left(-0.6 + \frac{m_{\text{WDM}}}{1 \text{ keV}} \right) h \text{ Mpc}^{-1}, \quad (10)$$

¹<https://github.com/ravi398/WDM>.

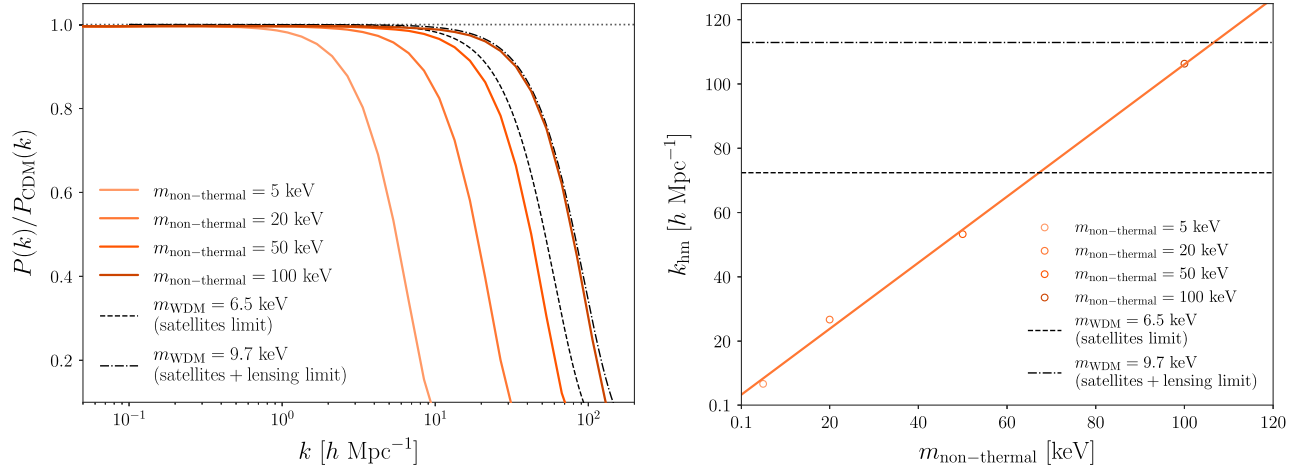


FIG. 2. Left: ratio of the linear matter power spectrum relative to CDM for our nonthermal warm dark matter model (red lines, with masses of 5 to 100 keV, from lightest to darkest colors). Black dashed and dot-dashed lines respectively show WDM transfer functions for 6.5 and 9.7 keV thermal relics, which are respectively ruled out at 95% confidence limits by analyses of the Milky Way satellite galaxy population [18] and its combination with strong lensing flux ratio statistics [36]. Right: the half-mode wave number, at which the linear matter power spectrum drops to 25% that in CDM, versus nonthermal warm dark matter particle mass. The solid red line shows the fit to our CLASS output given by Eq. (7); open circles show half-mode wave numbers derived from our CLASS output for the nonthermal models shown in the left panel. For reference, horizontal dashed (dot-dashed) lines show half-mode wave numbers for 6.5 (9.7) keV thermal-relic WDM models, respectively.

where m_{WDM} is the thermal-relic WDM mass. Comparing Eqs. (7) and (10), we obtain the following relation between m_{WDM} and $m_{\text{nonthermal}}$:

$$m_{\text{nonthermal}} = 12.2 \left(-0.9 + \frac{m_{\text{WDM}}}{1 \text{ keV}} \right) \text{ keV}. \quad (11)$$

We have verified that this relation is accurate over the entire range of nonthermal masses we consider by comparing the corresponding transfer functions. Along the initial cutoff, discrepancies between matched transfer functions are typically at the subpercent level; such deviations are not detectable in the datasets on which we base our constraints. Thus, Eq. (11) provides a means to robustly translate existing thermal-relic warm dark matter constraints to constraints on our nonthermal model.

Note that $m_{\text{nonthermal}}$ is significantly larger than the corresponding m_{WDM} based on Eq. (11). A similar result was found for hot dark matter in the nonthermal distribution under consideration [40]. This essentially follows from the fact that the nonthermal momentum distribution has a long tail toward high velocities (e.g., see Fig. 1). Thus, at a given redshift, nonthermal WDM particles in our model have a higher average velocity compared to thermal WDM particles, even for the same mass.

We can gain further insight into the relation between $m_{\text{nonthermal}}$ and m_{WDM} by calculating free-streaming length via

$$\lambda_{\text{fs}} = \int_0^{a_{\text{eq}}} \frac{\langle v(a) \rangle}{a^2 H(a)} da, \quad (12)$$

which respectively has contributions from the relativistic and nonrelativistic regimes given by

$$\lambda_{\text{fs}} = 2ct_0 a_{\text{nr}} + I.$$

Here, the nonrelativistic contribution I is given by

$$I = \int_{a_{\text{nr}}}^{a_{\text{eq}}} \frac{\langle v(a) \rangle}{a^2 H(a)} da,$$

where the average velocity is

$$\langle v(a) \rangle = \frac{\int_0^\infty v f(v) 4\pi v^2 dv}{\int_0^\infty f(v) 4\pi v^2 dv}.$$

For thermal-relic WDM, these integrals are analytically tractable assuming $H^2(a) = \Omega_m a^{-3} + \Omega_{\text{rad}} a^{-3} + \Omega_\Lambda$, where Ω_i are fractional energy densities and a is the scale factor. For nonthermal WDM, we solve the integral equations numerically to compute the free-streaming scale as a function of $m_{\text{nonthermal}}$. We have verified that the nonthermal and thermal-relic free-streaming scales match each other well along the relation given by Eq. (11).

IV. CONSTRAINTS FROM THERMAL RELIC WDM MAPPING

We derive constraints on our nonthermal model based on Eq. (11). In particular, we use the 95% confidence lower limits on thermal-relic WDM of 6.5 keV, derived from the Milky Way satellite galaxy population, and 9.7 keV, derived from its combination with strong lensing flux ratio statistics. These constraints are illustrated in Fig. 3 and

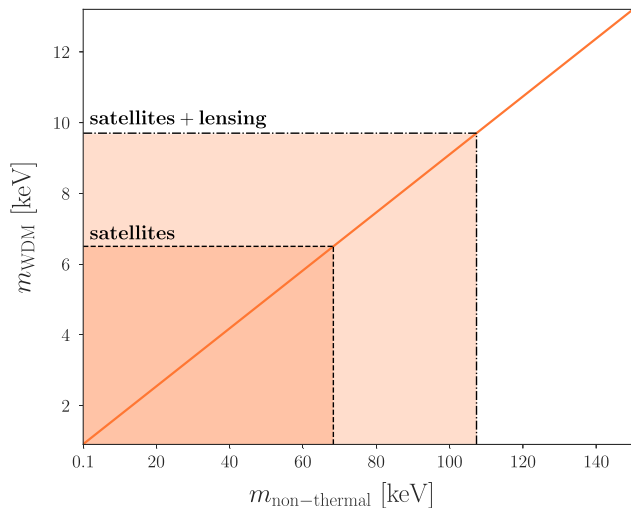


FIG. 3. Relation between nonthermal and thermal-relic WDM mass, and corresponding small-scale structure limits, derived by matching our nonthermal WDM linear matter power spectra to equivalent thermal-relic models. The solid red line shows the relation from Eq. (11); the dark and light shaded regions are respectively excluded at 95% confidence limits by the Milky Way satellite galaxy population and its combination with strong lensing flux ratio statistics.

map to lower limits on the nonthermal WDM mass of 68 and 107 keV, respectively. Following our calculation above, the corresponding free-streaming lengths are $\lambda_{\text{fs}} = 31$ kpc for $m_{\text{nonthermal}} = 107$ keV and $\lambda_{\text{fs}} = 29$ kpc for $m_{\text{WDM}} = 9.7$ keV. The latter value is in reasonable agreement with the fit in Ref. [47].

We emphasize that our nonthermal transfer functions are essentially identical to thermal-relic models, including for nonthermal masses at our 95% confidence limits (e.g., see the left panel of Fig. 2). Furthermore, there is no new, nonlinear physics introduced by our model: in both the nonthermal and thermal-relic WDM cases, suppression of structure formation relative to CDM is set by the free-streaming scale, which is imprinted well before matter-radiation equality. Thus, we expect nonlinear observables that drive the small-scale structure limits we map to, such as the halo and subhalo mass functions and mass-concentration relations, to be practically identical to those in thermal-relic WDM, which are well studied.

We note that the precise mapping between our nonthermal transfer functions and thermal-relic WDM at and below the cutoff scale justifies our use of combined Milky Way satellite and strong lensing limits. In particular, the lensing limits depend sensitively on halo concentrations [32,48], which are in turn sensitive to power on scales even smaller than k_{hm} .

V. CONCLUSIONS

We have derived small-scale structure limits on WDM produced via heavy scalar decay. This production

mechanism is theoretically motivated and yields a distinctly nonthermal primordial phase-space distribution. Nonetheless, assuming that the entire dark matter relic density is composed of these warm particles, we have shown that the resulting linear matter power spectra are nearly identical to thermal-relic WDM. We exploited this correspondence to derive a mapping between our nonthermal particle mass and the thermal-relic WDM mass. Confronting this model with observational constraints from Milky Way satellite galaxies and strong gravitational lensing yields a lower limit on the nonthermal particle mass of 107 keV at 95% confidence limits, which represents the most stringent lower limit to date (also see Ref. [49]).

The sensitivity of both small-scale structure probes we leveraged will improve significantly over the next decade. Specifically, the combination of next-generation observational facilities, including the Vera C. Rubin Observatory [50], and space telescopes, including the Nancy Grace Roman Space Telescope [51], is expected to probe most of the undiscovered Milky Way satellite galaxy population as well as faint dwarf galaxies throughout the local volume [52,53]. These same facilities will drastically increase the sample of strongly lensed systems available for deep follow-up observations necessary to derive dark matter constraints [54,55], and will also provide qualitatively new means of probing low-mass halos [56]. Together, these observations are expected to probe warm dark matter masses up to ~ 20 keV [52], which translate to nonthermal particles masses of ~ 200 keV for our production mechanism.

The forecasts above assume that warm dark matter particles compose the entire dark sector. Smaller fractions of lower-mass warm dark matter particles may evade next-generation constraints. Here, we have treated the parameters in our nonthermal distribution functions phenomenologically; however, it will be interesting to consider explicit realizations of this scenario that naturally yield mixed cold-plus-warm dark matter scenarios. In the context of string theory, two WDM production scenarios are particularly relevant: the decay of the inflaton to excitations at the bottom of a warped throat [57], or a hidden sector with keV-scale condensation (e.g., see Ref. [58]). A generic outcome of such string models is that dark matter can be mixed, with one component arising from the decay of a heavy modulus (as discussed in this paper) and the other corresponding to a thermal relic that freezes out from the Standard Model sector (see Ref. [59] for a recent review of various scenarios for dark matter in string theory). We plan to pursue detailed studies of these possibilities in future work.

APPENDIX: VARIATIONS IN NONTHERMAL PRODUCTION MECHANISM PARAMETERS

As discussed above, the distribution function for our nonthermal model is characterized by the mass of the heavy particle, m_ϕ , its decay rate, τ , and the branching ratio for decay to WDM, B_{sp} . Here, we explicitly check that

TABLE I. Variations of production mechanism parameters used for the test in Fig. 4. Note that m_{sp} is given in eV.

Model parameters	Case 1	Case 2	Case 3	Case 4	Case 5	Case 6
m_ϕ	$10^{-6}M_{\text{pl}}$	$10^{-8}M_{\text{pl}}$	$10^{-7}M_{\text{pl}}$	$10^{-8}M_{\text{pl}}$	$10^{-6}M_{\text{pl}}$	$10^{-8}M_{\text{pl}}$
τ	$10^8/m_\phi$	$10^9/m_\phi$	$10^8/m_\phi$	$10^8/m_\phi$	$10^8/m_\phi$	$10^9/m_\phi$
m_{sp}	5000	5000	5000	5000	5000	5000
B_{sp}	0.0118	0.0118	0.0118	0.0118	0.0218	0.0218

variations in these parameters do not strongly impact the linear matter power spectra that we use to construct a mapping to thermal-relic WDM. Specifically, we choose a set of variations as listed in Table I. The ratio of the linear matter power spectrum between parameter sets is shown in Fig. 4. We can see that power spectra are not strongly affected by these parameter variations, implying that our results are robust to specific choices regarding the details of our nonthermal WDM production mechanism.

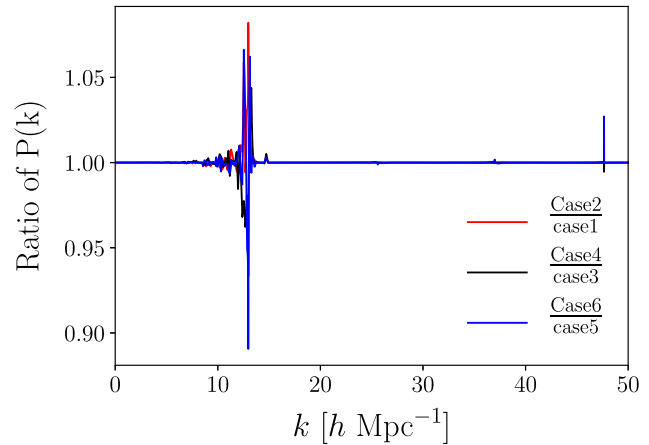


FIG. 4. Ratio of the linear matter power spectrum for sets of production mechanism parameter variations, as listed in Table I. The kinks that appear around $k = 12h \text{ Mpc}^{-1}$ are the result of small numerical artifacts in CLASS code; their location coincides with oscillations in nonthermal WDM power spectra at scales smaller than the initial cutoff.

- [1] S. Alam *et al.* (BOSS Collaboration), The clustering of galaxies in the completed SDSS-III baryon oscillation spectroscopic survey: Cosmological analysis of the DR12 galaxy sample, *Mon. Not. R. Astron. Soc.* **470**, 2617 (2017).
- [2] N. Aghanim *et al.* (Planck Collaboration), Planck 2018 results. VI. Cosmological parameters, *Astron. Astrophys.* **641**, A6 (2020); **652**, C4(E) (2021).
- [3] T. M. C. Abbott *et al.* (DES Collaboration), Dark energy survey year 3 results: Cosmological constraints from galaxy clustering and weak lensing, *Phys. Rev. D* **105**, 023520 (2022).
- [4] J. S. Bullock and M. Boylan-Kolchin, Small-scale challenges to the Λ CDM paradigm, *Annu. Rev. Astron. Astrophys.* **55**, 343 (2017).
- [5] A. A. Klypin, A. V. Kravtsov, O. Valenzuela, and F. Prada, Where are the missing Galactic satellites?, *Astrophys. J.* **522**, 82 (1999).
- [6] B. Moore, S. Ghigna, F. Governato, G. Lake, T. R. Quinn, J. Stadel, and P. Tozzi, Dark matter substructure within galactic halos, *Astrophys. J. Lett.* **524**, L19 (1999).
- [7] R. A. Flores and J. R. Primack, Observational and theoretical constraints on singular dark matter halos, *Astrophys. J. Lett.* **427**, L1 (1994).
- [8] B. Moore, Evidence against dissipationless dark matter from observations of galaxy haloes, *Nature (London)* **370**, 629 (1994).
- [9] M. Boylan-Kolchin, J. S. Bullock, and M. Kaplinghat, Too big to fail? The puzzling darkness of massive Milky Way subhaloes, *Mon. Not. R. Astron. Soc.* **415**, L40 (2011).
- [10] L. V. Sales, A. Wetzel, and A. Fattahi, Baryonic solutions and challenges for cosmological models of dwarf galaxies, *Nat. Astron.* **6**, 897 (2022).
- [11] J. R. Bond and A. S. Szalay, The collisionless damping of density fluctuations in an expanding universe, *Astrophys. J.* **274**, 443 (1983).
- [12] P. Bode, J. P. Ostriker, and N. Turok, Halo formation in warm dark matter models, *Astrophys. J.* **556**, 93 (2001).
- [13] S. Dodelson and L. M. Widrow, Sterile-Neutrinos as Dark Matter, *Phys. Rev. Lett.* **72**, 17 (1994).
- [14] K. Abazajian and S. M. Koushiappas, Constraints on sterile neutrino dark matter, *Phys. Rev. D* **74**, 023527 (2006).
- [15] A. Das, S. Das, and S. K. Sethi, Cosmological signatures of mass varying dark matter, [arXiv:2303.17947](https://arxiv.org/abs/2303.17947).
- [16] X.-D. Shi and G. M. Fuller, A New Dark Matter Candidate: Nonthermal Sterile Neutrinos, *Phys. Rev. Lett.* **82**, 2832 (1999).
- [17] A. De Gouvêa, M. Sen, W. Tangarife, and Y. Zhang, Dodelson-Widrow Mechanism in the Presence of Self-Interacting Neutrinos, *Phys. Rev. Lett.* **124**, 081802 (2020).
- [18] E. O. Nadler *et al.* (DES Collaboration), Milky Way Satellite Census. III. Constraints on Dark Matter Properties from Observations of Milky Way Satellite Galaxies, *Phys. Rev. Lett.* **126**, 091101 (2021).
- [19] I. A. Zelko, T. Treu, K. N. Abazajian, D. Gilman, A. J. Benson, S. Birrer, A. M. Nierenberg, and A. Kusenko, Constraints on Sterile Neutrino Models from Strong Gravitational Lensing, Milky Way Satellites, and the Lyman- α Forest, *Phys. Rev. Lett.* **129**, 191301 (2022).
- [20] R. An, V. Gluscevic, E. O. Nadler, and Y. Zhang, Can neutrino self-interactions save sterile neutrino dark matter?, [arXiv:2301.08299](https://arxiv.org/abs/2301.08299).
- [21] S. Bhattacharya, S. Das, K. Dutta, M. R. Gangopadhyay, R. Mahanta, and A. Maharana, Nonthermal hot dark matter from inflaton or moduli decay: Momentum distribution and

- relaxation of the cosmological mass bound, *Phys. Rev. D* **103**, 063503 (2021).
- [22] S. Das, A. Maharana, V. Poulin, and R. K. Sharma, Non-thermal neutrino-like hot dark matter in light of the S8 tension, *Phys. Rev. D* **105**, 103503 (2022).
- [23] A. Banerjee, S. Das, A. Maharana, and R. Kumar Sharma, Signatures of light massive relics on non-linear structure formation, *Mon. Not. R. Astron. Soc.* **516**, 2038 (2022).
- [24] T. Abbott *et al.* (DES Collaboration), The dark energy survey, [arXiv:astro-ph/1612.05560](https://arxiv.org/abs/1612.05560).
- [25] K. C. Chambers *et al.*, The Pan-STARRS1 surveys, [arXiv:1612.05560](https://arxiv.org/abs/1612.05560).
- [26] A. Drlica-Wagner, L. J. Kewley, J. R. Rigby, A. Acharyya, D. A. Berg, M. Bayliss, and K. Sharon (DES Collaboration), Milky Way satellite census. I. The observational selection function for Milky Way satellites in DES Y3 and Pan-STARRS DR1, *Astrophys. J.* **893**, 1 (2020).
- [27] E. O. Nadler *et al.* (DES Collaboration), Milky Way satellite census—II. Galaxy-halo connection constraints including the impact of the large magellanic cloud, *Astrophys. J.* **893**, 48 (2020).
- [28] K. Maamari, V. Gluscevic, K. K. Boddy, E. O. Nadler, and R. H. Wechsler, Bounds on velocity-dependent dark matter-proton scattering from Milky Way satellite abundance, *Astrophys. J. Lett.* **907**, L46 (2021).
- [29] S. Das and E. O. Nadler, Constraints on the epoch of dark matter formation from Milky Way satellites, *Phys. Rev. D* **103**, 043517 (2021).
- [30] D. V. Nguyen, D. Sarnaik, K. K. Boddy, E. O. Nadler, and V. Gluscevic, Observational constraints on dark matter scattering with electrons, *Phys. Rev. D* **104**, 103521 (2021).
- [31] S. Mau *et al.* (DES Collaboration), Milky Way satellite census. IV. Constraints on decaying dark matter from observations of Milky Way satellite galaxies, *Astrophys. J.* **932**, 128 (2022).
- [32] D. Gilman, X. Du, A. Benson, S. Birrer, A. Nierenberg, and T. Treu, Constraints on the mass-concentration relation of cold dark matter haloes with 11 strong gravitational lenses, *Mon. Not. R. Astron. Soc.* **492**, L12 (2020).
- [33] D. Gilman, Y.-M. Zhong, and J. Bovy, Constraining resonant dark matter self-interactions with strong gravitational lenses, *Phys. Rev. D* **107**, 103008 (2023).
- [34] A. Laroche, D. Gilman, X. Li, J. Bovy, and X. Du, Quantum fluctuations masquerade as halos: Bounds on ultra-light dark matter from quadruply-imaged quasars, *Mon. Not. R. Astron. Soc.* **517**, 1867 (2022).
- [35] V. Dike, D. Gilman, and T. Treu, Strong lensing constraints on primordial black holes as a dark matter candidate, *Mon. Not. R. Astron. Soc.* **522**, 5434 (2023).
- [36] E. O. Nadler, S. Birrer, D. Gilman, R. H. Wechsler, X. Du, A. Benson, A. M. Nierenberg, and T. Treu, Dark matter constraints from a unified analysis of strong gravitational lenses and Milky Way satellite galaxies, *Astrophys. J.* **917**, 7 (2021).
- [37] J. Hasenkamp and J. Kersten, Dark radiation from particle decay: Cosmological constraints and opportunities, *J. Cosmol. Astropart. Phys.* **08** (2013) 024.
- [38] J. P. Conlon and M. C. D. Marsh, The cosmophenomenology of axionic dark radiation, *J. High Energy Phys.* **10** (2013) 214.
- [39] C. Miller, A. L. Erickcek, and R. Murgia, Constraining nonthermal dark matter's impact on the matter power spectrum, *Phys. Rev. D* **100**, 123520 (2019).
- [40] S. Bhattacharya, S. Das, K. Dutta, M. R. Gangopadhyay, R. Mahanta, and A. Maharana, Nonthermal hot dark matter from inflaton or moduli decay: Momentum distribution and relaxation of the cosmological mass bound, *Phys. Rev. D* **103**, 063503 (2021).
- [41] J. Lesgourgues, The cosmic linear anisotropy solving system (CLASS) I: Overview, [arXiv:1104.2932](https://arxiv.org/abs/1104.2932).
- [42] J. Lesgourgues and T. Tram, The cosmic linear anisotropy solving system (CLASS) IV: Efficient implementation of non-cold relics, *J. Cosmol. Astropart. Phys.* **09** (2011) 032.
- [43] M. Viel, J. Lesgourgues, M. G. Haehnelt, S. Matarrese, and A. Riotto, Constraining warm dark matter candidates including sterile neutrinos and light gravitinos with WMAP and the Lyman-alpha forest, *Phys. Rev. D* **71**, 063534 (2005).
- [44] Q. Decant, J. Heisig, D. C. Hooper, and L. Lopez-Honorez, Lyman- α constraints on freeze-in and super-WIMPs, *J. Cosmol. Astropart. Phys.* **03** (2022) 041.
- [45] C. M. Vogel and K. N. Abazajian, Entering the era of measuring sub-galactic dark matter structure: Accurate transfer functions for axino, gravitino and sterile neutrino thermal warm dark matter, [arXiv:2210.10753](https://arxiv.org/abs/2210.10753).
- [46] E. O. Nadler, V. Gluscevic, K. K. Boddy, and R. H. Wechsler, Constraints on dark matter microphysics from the Milky Way satellite population, *Astrophys. J. Lett.* **878**, 32 (2019); **897**, L46(E) (2020).
- [47] A. Schneider, R. E. Smith, A. V. Maccio, and B. Moore, Nonlinear evolution of cosmological structures in warm dark matter models, *Mon. Not. R. Astron. Soc.* **424**, 684 (2012).
- [48] D. Gilman, A. Benson, J. Bovy, S. Birrer, T. Treu, and A. Nierenberg, The primordial matter power spectrum on sub-galactic scales, *Mon. Not. R. Astron. Soc.* **512**, 3163 (2022).
- [49] G. Ballesteros, M. A. G. Garcia, and M. Pierre, How warm are non-thermal relics? Lyman- α bounds on out-of-equilibrium dark matter, *J. Cosmol. Astropart. Phys.* **03** (2021) 101.
- [50] Ž. Ivezić *et al.* (LSST Collaboration), LSST: From science drivers to reference design and anticipated data products, *Astrophys. J.* **873**, 111 (2019).
- [51] D. Spergel *et al.*, Wide-field infrared survey telescope—astrophysics focused telescope assets WFIRST-AFTA 2015 report, [arXiv:1503.03757](https://arxiv.org/abs/1503.03757).
- [52] A. Drlica-Wagner *et al.* (LSST Dark Matter Group), Probing the fundamental nature of dark matter with the large synoptic survey telescope, [arXiv:1902.01055](https://arxiv.org/abs/1902.01055).
- [53] S. Gezari *et al.*, R2-D2: Roman and Rubin—from data to discovery, [arXiv:2202.12311](https://arxiv.org/abs/2202.12311).
- [54] M. Oguri and P. J. Marshall, Gravitationally lensed quasars and supernovae in future wide-field optical imaging surveys, *Mon. Not. R. Astron. Soc.* **405**, 2579 (2010).
- [55] C. Weiner, S. Serjeant, and C. Sedgwick, Predictions for strong-lens detections with the Nancy Grace Roman Space Telescope, *Res. Notes Am. Astron. Soc.* **4**, 190 (2020).

- [56] K. Pardo and O. Doré, Detecting dark matter subhalos with the Nancy Grace Roman Space Telescope, *Phys. Rev. D* **104**, 103531 (2021).
- [57] A. R. Frey, R. J. Danos, and J. M. Cline, Warped Kaluza-Klein dark matter, *J. High Energy Phys.* **11** (2009) 102.
- [58] J. Halverson and P. Langacker, TASI lectures on remnants from the string landscape, *Proc. Sci. TASI2017*, 019 (2018) [[arXiv:1801.03503](#)].
- [59] M. Cicoli, J. P. Conlon, A. Maharana, S. Parameswaran, F. Quevedo, and I. Zavala, String cosmology: From the early universe to today, [arXiv:2303.04819](#).